Disordered plane waves in the transition between target and antitarget patterns

Xujin Yuan,[1] Xiaochuan Lu,[1] Hongli Wang,[1,2,3] and Qi Ouyang[1,2,3,*]
[1]*State Key Laboratory for Mesoscopic Physics, Department of Physics, Peking University, Beijing 100871, China*
[2]*Center for Theoretical Biology, Peking University, Beijing 100871, China*
[3]*The Beijing-Hong Kong-Singapore Joint Center for Nonlinear and Complex Systems, Peking University (PKU), Beijing 100871, China*
(Received 1 September 2009; published 3 December 2009)

Since the experimental observation of antiwaves in reaction-diffusion (RD) systems, the discrepancy between the theoretical prediction and the experimental observation on the transition from inwardly rotating chemical waves to normal waves remains an unsolved problem. Theoretical predictions using both RD model and complex Ginzberg-Landau equation indicate that there exists a trend in which wave vector approaches to zero in the transition process, while disordered plane waves near the onset were observed in experiment. This discrepancy motivated us to conduct a systematic research to investigate the transition. Using chlorite-iodide-malonic acid reaction as model system and with a thorough parameter scanning, we found clear trend that the wave vector decreased near the transition point, where wavelength diverged. This observation is consistent with the theoretical predictions. However, disordered plane waves appeared in the region near the onset. Comparing the experimental results with the results from numerical simulation, we found that spatial inhomogeneity of the diffusion coefficient was the main cause of the disordered plane waves.

DOI: 10.1103/PhysRevE.80.066201 PACS number(s): 89.75.Kd, 82.40.Ck, 82.40.Bj, 47.54.−r

I. INTRODUCTION

Different from ordinary outwardly propagating spiral or concentric (target) chemical waves, the inwardly rotating spirals (antispirals) and the inwardly propagating concentric waves (antitarget) have a phase velocity direction opposite to their group velocity. Antiwaves were first observed by Vanag *et al.* in the Belousouv-Zhabotinsky (BZ) reaction that dispersed in water droplets of a water-in-oil AOT microemulsion (BZ-AOT system) [1–3]. Since then, a great deal of theoretical and numerical investigations has been carried out in order to understand the mechanism of antiwaves behavior [4,5]. Subsequently antispirals were discovered in other systems, such as other chemical systems [6,7]; an artificial tissue of oscillatory cells, which is very close to biological system [8]. In experimental studies, antitarget in a single-phase reaction-diffusion system was found [9]. The experimental research aimed at the transition process between antiwaves and normal waves was also reported [9].

Simulation and theoretical studies using complex Ginzberg-Landau equation (CGLE) and reaction-diffusion (RD) models indicate that antiwaves should exist in a system which is near the Hopf bifurcation [10,11]. Antiwaves will change into normal waves when the system is further away from the bifurcation point [12]. The pattern formation theory predicts that antiwaves and normal waves are distinguished only by the sign of the phase velocity of the emitted waves. So that, as the variation in a certain control parameter, the wave vector of the phase waves changes from a negative value to zero, then to a positive value. As a result, the transition from antiwaves to normal waves should be characterized by a divergence in the wavelength [13]. However, such theoretically predicted characteristic phenomenon has not been observed in any experiments. Instead, in the experiment of Ref. [9], disordered plan waves were observed. The regime of disordered pattern just seems to cover the region where the wavelength diverges. The reason of the appearance of disordered plane waves is not yet clear; it is suspected that the inhomogeneity of the experimental medium is one of the major causes [9].

In this paper, the transition between antiwaves and normal waves is investigated systemically and meticulously. The aim of this work is to resolve the discrepancy between the theoretical prediction and the experimental observation. To this end, both experiment and numerical simulation were conducted in this research.

II. EXPERIMENTAL OBSERVATION

Antispiral and antitarget were originally observed in the BZ-AOT system, which is a two-phase system mixed water with oil. Theoretical studies suggest that antiwaves should also exist in the single-phase RD system. Recently antitargets in a single-phase system were observed in the chlorite-iodide-malonic acid (CIMA) reaction [9], and a type of antiwave-wave exchange was witnessed: with the increase in a control parameter so that the system was further away from the Hopf onset, an antitarget was gradually pushed out by a normal spiral, which could not be explained by CGLE. It was also reported that the exchange between antiwaves and normal waves was accompanied by the appearance of disordered plane waves. Following this previous study, we used the CIMA reaction in our experimental investigation.

A typical spatially open reactor was used to conduct the experiment. The details of the reactor have been described in previous studies [14,15]. In brief, the reaction medium was a transparent disk of 1.25% agarose hydrogel, 2 mm in thickness, and 25 mm in diameter, pre-loaded with certain amount of polyvinyl alcohol (PVA), the color indicator of the reactant tri-iodide. Since the agarose-water solution was very

*Author to whom correspondence should be addressed; qi@pku.edu.cn

sticky, it was hard to make it melted with water uniformly. As a result, spatial inhomogeneity in gel density was inevitable in the experiment, which behaved as inhomogeneity in the diffusion constant of the reaction medium. Under normal conditions, the effect of this inhomogeneity is relatively small, and it does not influence the behavior of chemical waves. However, they could make a qualitative difference near the onset of wave-antiwave transition, as we will witness later.

The agarose gel was sandwiched between two porous glass disks which have an average pore size of 4 nm. The opposite two sides of porous glass disks were, respectively, in contact with two reactant reservoirs (I and II), where the reactants were continuously refreshed and kept homogeneous by magnetically stirring. The reactants diffused into glasses and met in the gel, where reactions took place. The temperature of the whole system was kept at 7.5 ± 0.5 °C. Plenty of time (two hours) was waited before the spatiotemporal patterns were recorded by a charge-coupled device camera, so that the system could reach its asymptotic state.

The experiments were carried out with two feeding solutions, respectively fed to two reservoirs. Solutions in both reservoirs contain 3.48 mM potassium iodide and 4.5 mM sodium sulfate. Beside this, one solution contained 20 mM sodium chlorite, 1 mM sodium hydroxide; the other contained 21 mM sulfuric acid, and malonic acid (MA), which served as one of the control parameters and varied from 5.7 mM to 12 mM in the experiments. The concentration of PVA in the reactor medium is another control parameter. Because of its molecular size, PVA diffuses very slowly in the reaction medium. This causes a decrease of the effective diffusion coefficient of activator (I^-) in the reaction system. As a result, if the PVA concentration is set high, Turing pattern [14,15] rather that traveling waves may appear in the experimental system. Previous experiment showed that when the PVA concentrate was above 9 g/L, Turing pattern dominated the system [16]. In this experiment, we kept the PVA concentration at 4 g/L, so the traveling waves were the only observed patterns.

At the beginning of the experiment, the control parameters were set beyond but near the critical point of the Hopf bifurcation ([MA]=5.7 mM). After some transient time, we observed that all chemical waves started to have a strong trend to move toward a wave source, which was located at the central area of the reaction medium. Gradually the waves formed round shape and an antitarget with smooth wave front shaped up, as shown in Fig. 1(a). The chemical waves came forth from the outskirts of the reaction medium, split, and formed up round wavefront. The wave front spread inwardly and finally faded away in the center. In the split process, a phenomenon similar to the accelerating waves that first observed by Vanag *et al.* [2] in the antispiral regime was found, in which the joint wave front accelerated before splitting into two wavefront [see the top-right corner of Fig. 1(a)].

In order to explore the transition process from antiwaves to normal waves, we raised the concentration of MA so that the system was gradually tuned away from the Hopf bifurcation point. We found that the antitarget area was quite narrow, with an approximate range of 0.4 mM. As the concentration of MA was increased inside this narrow region, there was a clear trend in which the wavelength of antitarget increased, as shown in Fig. 2. When the concentration of MA was increased across the antiwave region (above 6.0 mM), the antitarget began to deform in both central and periphery area, transforming into a state of disordered plane waves. Figure 1(b) provides an example of such a deform process. At [MA]=9.0 mM, the disordered plane waves dominated the whole reaction medium [Fig. 1(c)]. Unlike the ordinary plane wave, which has regular wave fronts and curvature of wavefront is nearly zero, the curvature of disordered plane waves was either positive or negative from place to place. This regime of the disordered plane wave occupied a wide parameter range compared to that of the antitarget. As the concentration of MA was increased even further (above 10.8 mM), normal target began to emerge [Fig. 1(d)], which eventually dominated the whole reaction medium.

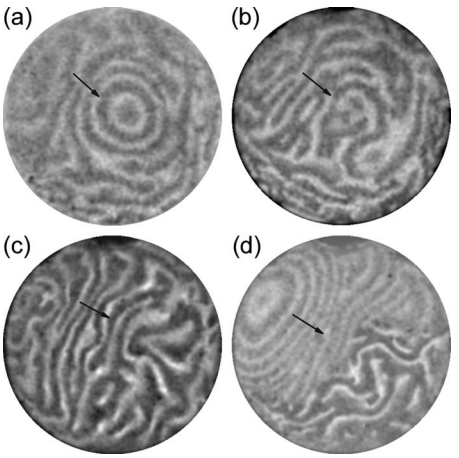

FIG. 1. Experimental results of the transition from antitarget to target. [MA] in (a) 5.8 mM, antitarget; (b) 6.0 mM, antitarget deformation; (c) 9.0 mM, disordered plane waves; and (d) 12 mM, target. View size diameter is 21.0 mm.

The wavelength of different traveling-wave patterns as a function of the control parameter is presented in Fig. 2. The behavior of waves can be divided into three areas: an antitarget area, a disordered plane-wave area, and a normal target

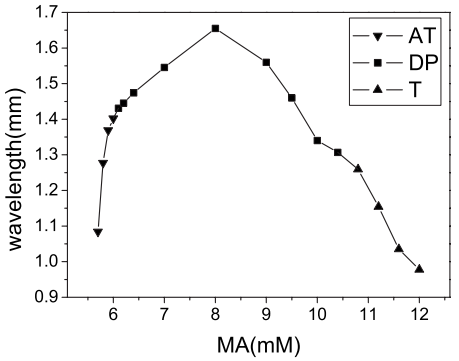

FIG. 2. Measured wavelength of the targets and disordered plane waves as the concentration of MA is tuned away from the Hopf onset. AT stands for antitarget; DP stands for disordered plane wave; T stands for target.

area. It is noticed in Fig. 2 that as the increase of the concentration of MA, the wavelength increases in the antitarget area and decreases in the target area. This behavior reflects the theoretical prediction of CGLE and RD model, in which the wave vector drops and approaches to zero in the transition between antiwaves and normal waves [13]. Besides, we found a region of the disordered plane waves which spanned a wide range in the transition process. It just covered up the peak where wavelength should diverges according to theoretical prediction. Moreover, we noticed that there was still a trend in which the wavelength of the disordered plane wave reached a maximum value at [MA]=8 mM. These observations cannot readily be explained by theory.

III. NUMERICAL SIMULATIONS

In order to resolve the discrepancy between experimental observations and the theoretical prediction, we conducted numerical simulation and compared the results with the experimental observations. The central idea for resolving the discrepancy is that the spatial inhomogeneity in the reaction medium may play an essential role near the onset of the wave-antiwave transition.

In the corresponding simulation and theoretical analysis, a version of the Lengel-Epstein model was selected, which can qualitatively describe the CIMA reaction [17–19]. Here we took the reaction of the color indicator PVA into account [20]:

$$S + I_3^- \leftrightharpoons C, \tag{1}$$

where S, I_3^-, and C represent, respectively, the concentration of PVA, tri-iodide, and PVA-iodide complex. This modification makes the comparison between experiments and numerical simulations more quantitative.

It is supposed that the above reaction is so fast that it is always in a quasiequilibrium. Under this assumption, the nondimensional form of Lengel-Epstein model can be written as

$$\partial x/\partial t = \delta[a - x - 4xy/(1+x^2)] + \delta D_x \nabla_r^2 x,$$

$$\partial y/\partial t = b[x - xy/(1+x^2)] + D_y \nabla_r^2 y, \tag{2}$$

where x and y are no-dimensional concentration of I^- and ClO_2^-; δ is related to the indicator's concentration: $\delta = 1/(1+SK) = 1/(1+C_0/X_0)$, where K is the equilibrium constant of reaction (1), C_0 and X_0 is, respectively, the average concentration of the PVA-iodide complex and iodide. According to Ref. [18], X_0 is between 10^{-4} M and 10^{-5} M. Considering the concentration of PVA (4 g/L), δ can be estimated as about 0.1.

There is a unique uniform steady-state solution in Eq. (2) given by $(x_0, y_0) = (a/5, 1+a^2/25)$. Linear stability analysis shows that the steady state becomes unstable and the system undergoes a Hopf bifurcation if $a > a_c = 5(b + \sqrt{b^2 + 60d^2})/6d$. The corresponding intrinsic Hopf frequency is $\omega_c = \sqrt{\frac{25a_c b}{25+a_c^2}}$ at the critical point. Using the reductive perturbation method, one can derive the corresponding CGLE

$$\frac{\partial W}{\partial t} = W - (1+i\alpha)|W|^2 W + (1+i\beta)\nabla_r^2 W, \tag{3}$$

where W is the amplitude of oscillation. The nonlinear dispersion coefficient α and linear dispersion coefficient β can be calculated [9,12]

$$\alpha = \frac{26x_0^6 - 119x_0^4 + 100x_0^2 - 75}{15\delta(3x_0^2 - 5)(2x_0^4 - 27x_0^2 - 5)}\omega_c,$$

$$\beta = \frac{D_x - D_y}{5\delta(D_x + D_y)}\omega_c. \tag{4}$$

According to former analysis [21], the phase velocity has the same sign as the wave vector, so that antiwaves change into normal waves when the wave vector is across zero. This result applies to both CGLE and RD model. In the CGLE model of Eq. (3), the antiwave-wave transition line is determined by $\alpha=\beta$, which is related to a, b, δ, D_x, D_y through Eq. (4). Plugging in the value of $b=0.37$, $\delta=0.1$ that are estimated from experiments, and $D_x=0.062$, $D_y=0.075$, which are approximate as in Ref. [18], the Hopf bifurcation should take place when $a>10.3$ and resulting patterns should be antiwaves. If one increases the value of a from the Hoft onset, the antiwave-wave transition should occur on $a=13.7$. All these values of a (corresponding to the dimensionless parameter of the concentration of MA) are right in the range of our control parameter in the experiments. We can thus conclude that the observed patterns in experiments occur around antiwave-wave transition, and model (2) can quantitatively describe the observed phenomena.

From the above experimental results, we know that the disordered plane waves take place just in the transition region between antiwave and normal wave. In this regime, the wave vector of the phase velocity change directions. Considering that there is inhomogeneity in diffusion constant in the experimental system (as stated in the previous section), according to Eq. (4) and the condition for the wave-antiwave transition ($\alpha=\beta$), this inhomogeneity will sure influence the local direction of the phase waves. As a result, near the transition point, local regions with opposite phase velocities can be expected to exist, which we think is the source of disordered plane waves. To verify this hypothesis, in the following we conducted systematic numerical simulations near the transition point.

In the numerical studies, a was chosen as the control parameter. The inhomogeneity was introduced to D_x and D_y to imitate the spatial inhomogeneity in the reaction medium, which was realized by adding a random value within a maximum disturbance strength (d) in the diffusion constants. In order to directly compare with the experimental observations, different strength of inhomogeneity (d) were tested for the effect of inhomogeneity on wave competitions. Numerical simulations were realized in a 256 by 256 grid, with spatial step of 4.0 and time step of 0.1. Equation (2) was integrated using the second-order Runge-Kutta method with no-flux boundary condition. In order to get a target pattern, a small inhomogeneous area that served as the target source was introduced in the center of the lattice. This target source

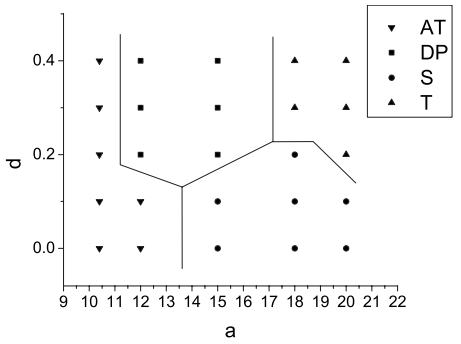

FIG. 3. Phase diagram using a and maximum strength of the spatial disturbance d as control parameters. AT, DP, S, and T stands for, respectively, antitarget, disordered plane waves, normal spiral, and normal target.

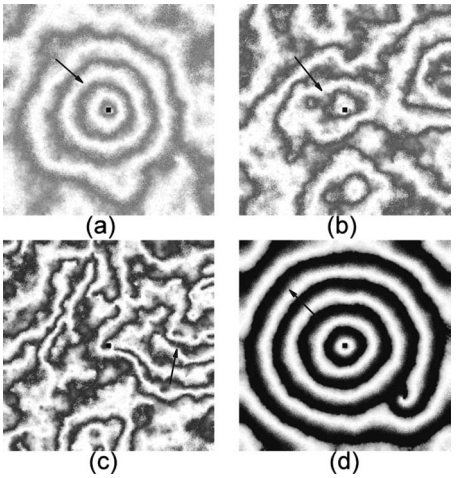

FIG. 4. Typical simulation results of dimensionless Lengyel-Epstein model. The value of a is, (a) 10.6, (b) 11.0, (c) 12.0, (d) 20.0. The system moves away from the Hopf onset as a increases. The other parameters are given in the text. The arrows point to the directions of phase wave movement.

was planted by selecting a small area (6 by 6 grids) and keeping the values of $x=0$ and $y=0$ inside it. Under these conditions and with a crossed the value of Hopf bifurcation point, we observed that as the simulation evolved from an initial condition, the antitarget gradually suppressed the antispiral and finally won out, as shown in Fig. 4(a).

The phase diagram of Fig. 3 summarizes the simulation results. At low disturbance strengths, an antitarget changes to a normal spiral at the onset of antiwave-wave transition. The behavior of the transition agrees with the theoretical prediction and numerical study of Refs. [9,12]. The pattern selection is attributed to wave competition between target and spiral: for normal waves, spiral suppresses target because of a bigger oscillation frequency; for antiwaves, antitarget dominates the antispiral because of a smaller oscillation frequency. In the latter case, wave fronts with a large period takes more time to disappear into the wave source, which gives it an advantage in the pattern competition, so that the transition between antitarget and normal spiral is witnessed. At high disturbance strengths, however, the behavior of the system changes dramatically. As the increase in the control parameter a, antitarget undergoes a transition to a pattern of disordered plane waves, then to a normal target.

Figure 4 provides four typical patterns in this scenario under high disturbance strength ($d=0.4$). Starting from an antitarget pattern [Fig. 4(a)], as the control parameter a was increased, antitarget transformed into disordered plane waves. Figure 4(b) gives a snap-shot of antitarget deformation, and Fig. 4(c) shows the disordered plane waves appearance. Agreeing with the experimental observations, these simulation results show that disordered plane waves cover up the area where, according to mean-field model of Eq. (3), the wave vector should approach to zero. The disordered plane waves had a coincident wave direction, but it was characterized by its wrinkled and thorny wave front, which was different from the regular plane wave. This type of wave should be attributed to the disturbance on the diffusion coefficient, which caused positive and negative phase velocity distribution from area to area.

At an even higher value of the control parameter a, a normal target dominated the whole area of RD system, as shown in Fig. 4(d). We noticed that target waves tended to win over spiral under high inhomogeneity strength in the normal wave area. In order to understand this phenomenon, We calculated the period of spirals and target patterns as a function of the inhomogeneity strength d. At typical normal wave area ($a=20$), as d rose from 0.1 to 0.2, the period of spiral increased from 34.50 to 37.40 while period of target slightly dropped from 34.59 to 34.50. Since in the normal wave regime, patterns with higher frequencies always win [22], this explains the reason why targets outrun spirals under high inhomogeneity condition. In this regime, the effect of inhomogeneity in the diffusion constant becomes secondary because all the local waves become normal waves; the variation in diffusion constant can be smoothed out by the diffusion itself.

IV. DISCUSSION AND CONCLUSION

Different from the former theoretical predictions, our experiments show that disordered plane waves appear near the antiwave-wave transition. This observation is confirmed by our numerical simulation that introducing inhomogeneity in the diffusion constant to the RD model. We thus conclude that the discrepancy between the former theory and experiment is due to the spatial fluctuations of diffusion constants in the system. To further verify this hypothesis, we checked the wavelength of the patterns as a function of the control parameter in the simulation. We predict that outside the disordered plane-wave region, the wavelength of antitarget, and normal target should increase as the control parameter approaches the transition point. In order to testify this prediction, a particular parameter scanning was carried out to find the variation trend of the wavelength, under the disturbance strength where the typical disordered plane wave can be generated ($d=0.4$). The result is shown in Fig. 5. One observes that it is quite similar to the experimental result: as the system gradually moves away from the Hopf bifurcation point to the antiwave-wave transition point, a quite narrow antitarget region first appears, with a clear trend in which the wave-

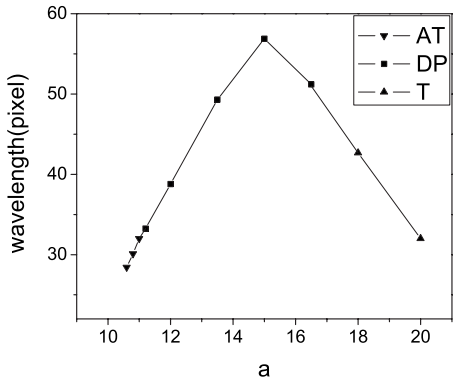

FIG. 5. Wavelength of patterns as a function of the control parameter obtained in the numerical simulation. A qualitatively agreement is reached compared to the experimental measurement.

length becomes larger. Then the wide region in which disordered plane wave comes, where wavelength reaches its maximum and fell down. This reflects the trend in which the wavelength diverges in a certain extent. When system is out of the region of disordered plane waves, normal target appears with a trend of wavelength dropping.

In summary, our research focused on the antiwave-wave transition in RD system. Through systematical studies in experiments using CIMA reaction and theoretical analysis and numerical simulations using Lengyel-Epstein model, we resolved the discrepancy between the former theoretical prediction and experimental observations. We proved that the absence of wavelength diversity that predicted in the former theoretical analysis and the appearance of the disordered waves that observed in the experiment were due to phase velocity diversity near the antiwave-wave transition point, which is caused by spatial inhomogeneity of diffusion constants. The disordered plane waves have a character of spatiotemporal chaotic pattern, but is not related with defect-mediated turbulence [15,23]. Moreover, we found that high inhomogeneity strength depress the frequency of spiral, helps the target to suppress the spiral.

ACKNOWLEDGMENTS

This work is partially supported by the NSF of China (Grant No. 10721403), the MOST of China (Grant No. 2009CB918500), and the National Basic Research Program of China (Grants No. 2006CB910706 and No. 2007CB814800). X.L. thanks the National Foundation for Fostering Talents of Basic Science (Grant No. J0630311) and Jun-Zheng Foundation at Peking University for support.

[1] V. K. Vanag and I. R. Epstein, Science **294**, 835 (2001).
[2] V. K. Vanag and I. R. Epstein, Phys. Rev. Lett. **87**, 228301 (2001).
[3] V. K. Vanag and I. R. Epstein, Phys. Rev. Lett. **88**, 088303 (2002).
[4] C. Wang, C. X. Zhang, and Q. Ouyang, Phys. Rev. E **74**, 036208 (2006).
[5] A. Rabinovitch, M. Gutman, and I. Aviram, Phys. Rev. Lett. **87**, 084101 (2001).
[6] A. Piel, V. Nosenko, and J. Goree, Phys. Rev. Lett. **89**, 085004 (2002).
[7] J. Wolff, M. Stich, C. Beta, and H. H. Rotermund, J. Phys. Chem. B **108**, 14282 (2004).
[8] H. Skødt and P. G. Sørensen, Phys. Rev. E **68**, 020902(R) (2003).
[9] X. Shao, Y. B. Wu, J. Z. Zhang, H. L. Wang, and Q. Ouyang, Phys. Rev. Lett. **100**, 198304 (2008).
[10] Y. Gong and D. J. Christini, Phys. Rev. Lett. **90**, 088302 (2003).
[11] H. L. Wang and Q. Ouyang, Chin. Phys. Lett. **21**, 2255 (2004).
[12] X. Shao, Y. Ren, and Q. Ouyang, Chin. Phys. B **15**, 513 (2006).
[13] E. M. Nicola, L. Brusch, and M. Bär, J. Phys. Chem. B **108**, 14733 (2004).
[14] Q. Ouyang and H. L. Swinney, Nature (London) **352**, 610 (1991).
[15] Q. Ouyang and H. L. Swinney, Chaos **1**, 411 (1991).
[16] X. J. Yuan, X. Shao, H. M. Liao, and Q. Ouyang, Chin. Phys. Lett. **26**, 024702 (2009).
[17] I. Lengyel, G. Rabai, and I. R. Epstein, J. Am. Chem. Soc. **112**, 9104 (1990).
[18] I. Lengyel and I. R. Epstein, Science **251**, 650 (1991).
[19] I. Lengyel, S. Kadar, and I. R. Epstein, Phys. Rev. Lett. **69**, 2729 (1992).
[20] B. Rudovics, E. Barillot, P. W. Davies, E. Dulos, J. Boissonade, and P. De Kepper, J. Phys. Chem. A **103**, 1790 (1999).
[21] P. S. Hagan SIAM J. Appl. Math. **42**, 762 (1982).
[22] C. X. Zhang, H. M. Liao, L. Q. Zhou, and Q. Ouyang, J. Phys. Chem. B **108**, 16990 (2004).
[23] Q. Ouyang and J. M. Flesselles, Nature (London) **379**, 143 (1996).